Computational Materials Science 150 (2018) 259–264

Contents lists available at ScienceDirect

Computational Materials Science

journal homepage: www.elsevier.com/locate/commatsci

Theoretical exploring the mechanical and electrical properties of *t*I12-$B_6C_4O_2$

Chao Liu[a,*], Mingwei Chen[b], Yi Yang[a], Jian Li[c], Cancan Shao[d], Penghui Li[d], Lingyu Liu[d], Julong He[d], Tongxiang Liang[a,*]

[a] School of Materials Science and Engineering, Jiangxi University of Science and Technology, Ganzhou 341000, China
[b] Institute of Engineering Research, Jiangxi University of Science and Technology, Ganzhou 341000, China
[c] College of Physics and Electronic Information Engineering, Qinghai Normal University, Xining 810000, China
[d] State Key Laboratory of Metastable Materials Science and Technology, Yanshan University, Qinhuangdao 066004, China

ARTICLE INFO

Keywords:
B—C—O
Anisotropy
Mechanical property
Electronic property
First principles

ABSTRACT

Utilizing the crystal structure prediction method (CALYPSO), a tetragonal B—C—O compound (*t*I12-$B_6C_4O_2$ with $I\bar{4}m2$ symmetric structure) was predicted. Computed formation enthalpies, elastic constants and phonon dispersion spectra certify that *t*I12-$B_6C_4O_2$ is thermodynamically, dynamically and mechanically stable. Our results indicate that *t*I12-$B_6C_4O_2$ has large mechanical moduli and high hardness (21.9 GPa). The directional dependences of the Young's modulus, shear modulus and Poisson's ratio have been visualized to analysis the mechanical anisotropy. The calculated band structure and partial density of state revealed that *t*I12-$B_6C_4O_2$ is a typical for conductor with sp^3 hybrid B—C and B—O covalent bonds.

1. Introduction

Since the B—C—O compounds ($B_6C_{1.1}O_{0.33}$ and $B_6C_{1.28}O_{0.31}$) have been synthesized for the first time via the high-pressure technology in the year 1997 [1,2], B—C—O compounds have walked into the field of scientific research. In 2001, boron suboxycarbide $B(C,O)_{0.1555}$ has first prepared by the reaction between B_4C and B_2O_3 compounds with 1:1 ratio at 5.5 GPa and 1400 K [3]. All the B—C—O compounds that have been synthesized are all non-stoichiometric ratio compounds, however, the research of the stoichiometric ratio B—C—O compounds has never been given up.

With the increasing perfection of computational materials science, the research of B—C—O compounds has been turned into theoretical aspects. As the simplest ternary compound in the B—C—O compounds and is isoelectronic with diamond, the potential structures of B_2CO were explored by Li et al. [4]. Two B_2CO polycrystalline structures (*t*P4-, and *t*I16-B_2CO) with superhard and semi-conduction nature were presented. Li suggested that in B—C—O compounds, such as B_2C_XO (X = 2, 3…), the increased C content will lead to more sp^3 C-C bonds, the compounds will be more harder [4], which has been verified by Zhang et al. [5]. Zhang et al. have introduced three diamond-like B_2C_XO (X ≥ 2) phases ($I4_1/amd$-B_2C_2O, $I\bar{4}m2$-B_2C_3O, and $P\bar{4}m2$-B_2C_5O). By evaluating the trends of mechanical property as a function of the C content, Zhang also discovered that the large C content is benefit to improve mechanical property of B_2C_XO compounds including elastic moduli and ideal strengths [5]. After explored the B—C—O system, Wang et al. first proposed a superhard B_4CO_4 phase, unlike the presented B—C—O compounds, which is nonisoelectronic with diamond [6]. The mechanical and electronic properties of B_4CO_4 have been systematically explored [7,8], and the domination strength is found as 27.5 GPa along the (0 0 1)⟨1 0 0⟩ slip system, demonstrating that B_4CO_4 is not intrinsically superhard, but is indeed a hard material [7]. Inspired by all superhard B_2C_XO (X ≥ 1) have the crystal structures similar to the allotropes of carbon, such as diamond and lonsdaleite, Liu et al. proposed two superhard B_2CO phases which derived from Cco-C8 and Bct-C4 [9]. Although all the proposed superhard B_2C_XO (X ≥ 1) phases and pseudo superhard B_4CO_4 are tetragonal structures, a lonsdaleite-like superhard B_2CO with nontetragonal structure was proposed [10], which broadened the structural system of B—C—O compounds. Up to this day, B—C—O compounds attracted increasing attention on not only three dimensional (3D) materials but also 2D materials. Zhou and Zhao discovered that the 2D B—C—O compounds are promising electronic devices [11]. The 2D B—C—O systems can be either metals or semiconductors depending on the B:O ratio (1:1 and 3:1, metallic; 2:1, semiconductive with a band gap range of 1.0 eV–3.9 eV [11].

In present work, through the analysis of the elastic constants and phonon spectra, a new B—C—O compound with chemical formula $B_6C_4O_2$ and space group $I\bar{4}m2$ was proposed. Then its mechanical and

* Corresponding authors.
E-mail addresses: liuchao198967@126.com (C. Liu), liang_tx@126.com (T. Liang).

https://doi.org/10.1016/j.commatsci.2018.04.020
Received 21 December 2017; Received in revised form 12 March 2018; Accepted 8 April 2018
Available online 20 April 2018
0927-0256/ © 2018 Published by Elsevier B.V.

electronic properties are researched, and the mechanical anisotropy has been explored systematically.

2. Computational methods

Adopting the CALYPSO code [12–14], the potential B—C—O polymorphs' structures with unfixed stoichiometric ratio were explored at ambient pressure. Once the structures were generated from the CALYPSO, geometric optimization, elastic constants and phonon frequency calculation, and physical properties research were implemented in CASTEP code [15]. The local density approximation was employed as the exchange correlation potential, which was calculated by the CA-PZ functional [16,17]. Geometric optimization was performed by BFGS minimization algorithm [18] with the following criteria were satisfied: (1) the force on atom is less than 0.01 eV/Å; (2) the atoms' displacement is below 5×10^{-4} Å; (3) the energy change does not go beyond 5×10^{-6} eV/atom; (4) the stress component does not exceed 0.02 GPa. The atomic electronic configuration was described by the norm conserving pseudopotential [19] with an energy cutoff of 960 eV. To ensure calculation precision at 1 meV, the k-points for Monkhorst − Pack grid was generated by a k-point separation ($2\pi \times 0.04$ Å^{-1}).

To ensure that the obtained structures were mechanically and dynamically stable, the elastic constants and phonon frequency throughout the Brillouin zone are calculated. For the elastic constants, we applied the efficient stress–strain method within CASTEP code and adopted the maximum strain amplitude 0.003 and 9 steps for each strain. For the phonon frequency, we employed the ultrasoft pseudopotential [18] and finite displacement method [20] with the primitive cells.

3. Results and discussion

3.1. Optimization of crystal structures

A wide selection of candidate structures of B—C—O compounds with variable stoichiometric ratios was calculated. In addition to the studied structures within compounds as B_2C_XO (X = 1, 2, 3, 5) and B_4CO_4, a new B—C—O compound were emerged from the thousands of candidate structures. It is a body-centered (1/2, 1/2, 1/2) tetragonal crystal structure with two formula units (f.u.) in unit cell, and possess the Laue class 4/*mmm* and point group $\bar{4}2m$. This one we proposed is $B_6C_4O_2$ with space group $I\bar{4}m2$ with 12 atoms per unit cell, denoted as *t*I12-$B_6C_4O_2$ (Fig. 1). All C atoms in *t*I12-$B_6C_4O_2$ are combined with four B atoms and formed [CB_4] tetrahedra, all O atoms are combined with four B atoms to form [OB_4] tetrahedra, indicating that there no C-O bonds in *t*I12-$B_6C_4O_2$. At ambient pressure, the optimized lattice parameters of *t*I12-$B_6C_4O_2$ are a = 2.617 Å, c = 11.226 Å with boron occupying 4*f* (0, 0.5, 0.587) and 2*c* (0, 0.5, 0.25) Wyckoff positions, carbon taking up 4*e* (0, 0, 0.341) Wyckoff position and oxygen occupying 2*a* (0, 0, 0) Wyckoff position.

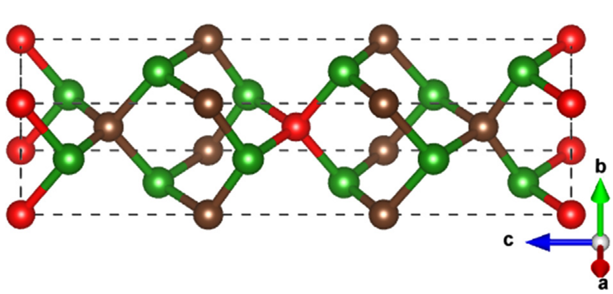

Fig. 1. Structure graphs for *t*I12-$B_6C_4O_2$. The balls in green, gray and red represent the B, C and O atoms, respectively.

3.2. Stability analysis

For tetragonal crystal system with Laue class 4/*mmm*, the necessary and sufficient conditions for elastic stability [21] are listed as Eq. (1).

$$C_{44} > 0,\ C_{66} > 0,\ C_{11} > |C_{12}|,\ (C_{11} + C_{12})C_{33} > 2C_{13}^2; \tag{1}$$

Here, the calculated independent elastic constants C_{ij}s at ambient pressure are C_{11} = 538.3 GPa, C_{33} = 557.0 GPa, C_{44} = 219.1 GPa, C_{66} = 120.3 GPa, C_{12} = 152.8 GPa and C_{13} = 164.8 GPa. The C_{ij}s satisfy the criteria above, declaring that *t*I12-$B_6C_4O_2$ possesses mechanical stability.

The existence of imaginary frequency denotes the dynamical instability and will cause distortion of crystal. Phonon dispersion of *t*I12-$B_6C_4O_2$ at ambient pressure is calculated and plotted in Fig. 2a. There are no soft phonon modes in entire Brillouin zone, suggesting it's dynamically stable.

For further experimental synthesis, there is necessity to explore the thermodynamic stability of *t*I12-$B_6C_4O_2$, which with respect to the separate phases as a function of pressure and can be quantified in the form of the formation enthalpies (ΔH):

$$\Delta\ \mathrm{H} = \mathrm{H}(B_6C_4O_2) - 6\mathrm{H}(B) - 4\mathrm{H}(C) - 2\mathrm{H}(O); \tag{2}$$

The α-B, graphite, and α-O_2 [22] are selected as the reference reactants. As exhibited Fig. 2b, the formation enthalpy decreases with the pressure increase and is always negative, which indicates the thermodynamic stability of *t*I12-$B_6C_4O_2$ and increasing pressure is be beneficial to synthesize *t*I12-$B_6C_4O_2$ through the path mentioned above.

3.3. Mechanical properties

The pressure-volume curves of *t*I12-$B_6C_4O_2$ are fitted by Birch-Murnaghan equation of state (BM-EOS) [23].

$$P(V) = 1.5B_0[(V/V_0)^{-7/3} - (V/V_0)^{-5/3}]\{1 + 0.75(B_0' - 4)[((V/V_0)^{-2/3} - 1]\}; \tag{3}$$

Herein, V_0 and V represent the volume per formula unit at zero pressure and given pressure; B_0 and B_0' represent the isothermal bulk modulus and its first pressure derivative. The fitting results and a series value of pressure versus volume are presented in Fig. 3. The obtained values of B_0 (GPa), B_0' and V_0 (Å^3) are listed as an interpolation table in Fig. 3.

Based on the elastic constants, the bulk modulus (B) and shear modulus (G) are calculated (288.6 GPa and 183.9 GPa, respectively). The value of B agrees well with the fitted value B_0 derived from the BM-EOS, declaring the calculation is correct and accurate. And then via Eq. (4), Young's modulus (E) and Poisson's ratio (ν) are obtained (455.1 GPa and 0.237, respectively). The results reveal that *t*I12-$B_6C_4O_2$ has high mechanical moduli, suggesting *t*I12-$B_6C_4O_2$ maybe a hard material. As one basic physical property of solid material, the hardness of *t*I12-$B_6C_4O_2$ is calculated based on Chen's empirical scheme [24] in accordance with Eq. (5).

$$\mathrm{E} = 9\mathrm{BG}/(3B + G); \nu = (3B - 2G)/(6B + 2G); \tag{4}$$

$$H_V = 2(\kappa^2 G)^{0.585} - 3; \kappa = G/B; \tag{5}$$

The calculation of mechanical properties demonstrates that *t*I12-$B_6C_4O_2$ is indeed a hard material with hardness 21.9 GPa.

Elasticity anisotropy is important for understanding the microcracks produced in ceramic materials and significantly influences materials' engineering application [25]. As a widely used criterion, the degree of anisotropy in the bonding between atoms in different planes can be measured by the shear anisotropy. The shear anisotropic factors [26] A_1, A_2 and A_3 are described for shear planes {1 0 0} between ⟨0 1 1⟩ and ⟨0 1 0⟩ directions, {0 1 0} between ⟨1 0 1⟩ and ⟨0 0 1⟩, {0 0 1} between ⟨1 1 0⟩ and ⟨0 1 0⟩, respectively.

For a tetragonal structure,

$$A_1 = A_2 = 4C_{44}/(C_{11} + C_{33} - 2C_{13}); A_3 = 2C_{66}/(C_{11} - C_{12}); \tag{6}$$

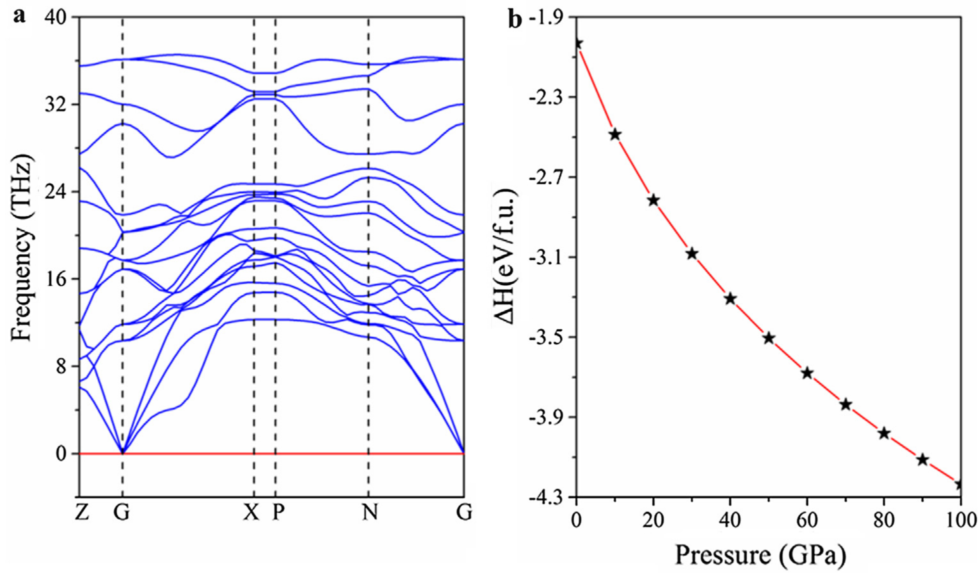

Fig. 2. The phonon dispersion spectra at ambient pressure (a) and formation enthalpy as a function of pressure (b) for $tI12$-$B_6C_4O_2$.

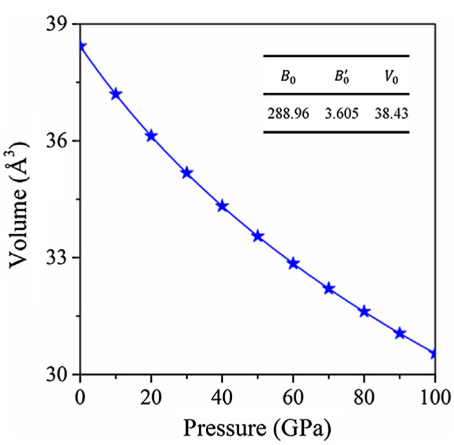

Fig. 3. Volume (per f.u.) of $tI12$-$B_6C_4O_2$ as a function of pressure. The scatter symbol and solid lines represent the calculated data and fitting results, respectively.

For the isotropic crystals, $A_1 = A_2 = A_3 = 1$. Any value deviation from 1 indicates the degree of shear anisotropy. Our calculated shear anisotropic factors ($A_1 = A_2 = 1.144$; $A_3 = 0.624$) illustrate that $tI12$-$B_6C_4O_2$ has the largest degrees of anisotropy of the {0 0 1} shear planes between ⟨1 1 0⟩ and ⟨0 1 0⟩ directions.The Young's modulus is defined as the ratio of stress to strain (both in the direction of applied load), and the shear modulus is the ratio of shear stress to linear shear strain. The Poisson's ratio can be expressed as the proportion of transverse strain (perpendicular to the applied load) and axial strain (in the direction of the applied load). The uniaxial stress can be described as a unit vector, and represented by two angles (θ, φ), we choose it as the first unit vector in the new basis set α. The measurement of other elastic properties (shear modulus, the Poisson's ratio) requires another unit vector β, normal to unit vector α and described by the angle ω. It is fully characterized by three angles (θ, φ and ω). The coordinates of these vectors are presented in Eq. (7), and $\alpha_1^2 + \alpha_2^2 + \alpha_3^2 = 1; \beta_1^2 + \beta_2^2 + \beta_3^2 = 1$.

$$\left|\begin{array}{c} \alpha_1 = \sin\theta\cos\varphi \\ \alpha_2 = \sin\theta\sin\varphi \\ \alpha_3 = \cos\theta \end{array}\right| ; \left|\begin{array}{c} \beta_1 = \cos\theta\cos\varphi\cos\omega - \sin\varphi\sin\omega \\ \beta_2 = \cos\theta\sin\varphi\cos\omega + \cos\varphi\sin\omega \\ \beta_3 = -\sin\theta\cos\omega \end{array}\right| \tag{7}$$

The Young's modulus and the Poisson's ratio can be expressed as [27]:

$$E(\theta,\varphi) = 1/S'_{11}(\theta,\varphi) = 1/N; \tag{8}$$

$$\nu(\theta,\varphi,\omega) = -S'_{12}(\theta,\varphi,\omega)/S'_{11}(\theta,\varphi) = -M/N; \tag{9}$$

with

$$M = S_{11}(\alpha_1^2\beta_1^2 + \alpha_2^2\beta_2^2) + S_{12}(\alpha_1^2\beta_2^2 + \alpha_2^2\beta_1^2) + S_{13}(\alpha_1^2\beta_3^2 + \alpha_3^2\beta_1^2 + \alpha_3^2\beta_2^2 + \alpha_2^2\beta_3^2) + S_{33}\alpha_3^2\beta_3^2 + S_{44}(\alpha_2\alpha_3\beta_2\beta_3 + \alpha_1\alpha_3\beta_1\beta_3) + S_{66}\alpha_1\alpha_2\beta_1\beta_2; \tag{10}$$

$$N = (\alpha_1^4 + \alpha_2^4)S_{11} + \alpha_3^4 S_{33} + \alpha_1^2\alpha_2^2(2S_{12} + S_{66}) + \alpha_3^2(1-\alpha_3^2)(2S_{13} + S_{44}); \tag{11}$$

The shear modulus [27] is acquired by loading a pure shear stress in the vector form, and expressed as Eq. (12).

$$1/G(\theta,\varphi,\omega) = 4S_{11}(\alpha_1^2\beta_1^2 + \alpha_2^2\beta_2^2) + 4S_{33}\alpha_3^2\beta_3^2 + 8S_{12}\alpha_1\alpha_2\beta_1\beta_2 + S_{66}(\alpha_1\beta_2 + \alpha_2\beta_1)^2 + 8S_{13}(\alpha_2\alpha_3\beta_2\beta_3 + \alpha_1\alpha_3\beta_1\beta_3) + S_{44}[(\alpha_2\beta_3 + \alpha_3\beta_2)^2 + (\alpha_1\beta_3 + \alpha_3\beta_1)^2]; \tag{12}$$

S_{ij} (i,j = 1..6) are the elastic compliance constants [28].

The Young's modulus in a given direction can be quantified by the distance from the origin of coordinate system to this surface. For an ideal isotropic matter, this 3D surface should be a sphere, however, $tI12$-$B_6C_4O_2$ exhibits an obvious anisotropy in Fig. 4.

The analytical formulas of Young's modulus E along tensile axes within specific planes including (0 0 1), (1 0 0), and (1 $\bar{1}$ 0) specific planes, are deduced from Eq. (8) and Eq. (11) and then summarized in Table 1, where τ is the angle between the principal crystal direction of the tensile plane and the tensile stress. The orientation dependences of Young's modulus E along tensile axes within (0 0 1), (1 0 0), and (1 $\bar{1}$ 0) specific planes are presented in Fig. 5. It is clear that the largest value of Young's modulus in $tI12$-$B_6C_4O_2$ is 513 GPa when the tensile axis is in the [0 1 1] direction, the minimal value of 342 GPa is along the [1 1 0] direction. From Fig. 5, we can conclude that the ordering of Young's modulus when the tensile axis along the principal crystal direction as: E[1 1 0] < E[1 0 0] < E[0 0 1] < E[1 1 1] < E[0 1 1].

Fig. 6 presents the directional dependences of Poisson's ratio ν. It can be found that the smallest value of Poisson's ratio in $tI12$-$B_6C_4O_2$ is 0.233 with the [1 0 0] direction, and the Poisson's ratio value of 0.240 is along the [0 0 1] direction. However the [1 1 0] directions hold the

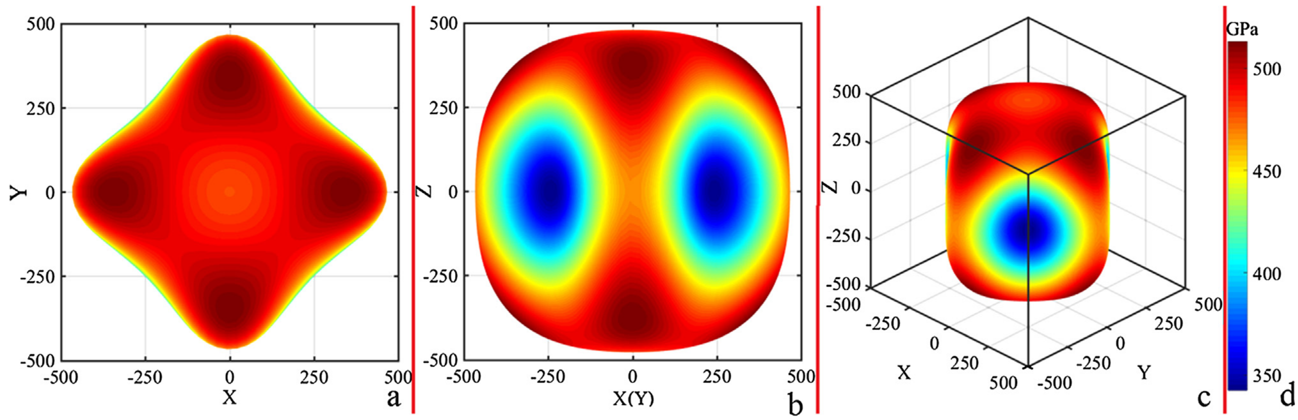

Fig. 4. Directional dependence of Young's moduli in tI12-$B_6C_4O_2$. a, b and c represent the XY plane views, ZX plane views and the stereo view, respectively. d represents the color map legend.

larger Poisson's ratio value, which is obviously exceeding 0.333 (A critical value for ductility/brittleness). It is an amusing thing that tI12-$B_6C_4O_2$ can be acted as a ductility material along the [1 1 0] direction, and as a brittleness material with the directions [1 0 0] and [0 0 1].

For a given shear plane, Eq. (12) can be simplified depending on the orientation angle τ between the shear stress direction and the specified crystal direction. The derived formulas of shear moduli along the (0 0 1), (1 0 0), and (1 $\bar{1}$ 0) shear planes are exhibited in Table 2. The orientation dependences of the shear moduli of tI12-$B_6C_4O_2$ are hence displayed in Fig. 7 for the shear (0 0 1), (1 0 0), and (1 1 0) planes. Obviously, the shear modulus within the (0 0 1) basal plane is free from influence of the orientation angle τ, which results from the fact that the formula of the shear modulus within the (0 0 1) basal plane is $G(0\,0\,1) = S_{44}^{-1} = C_{44} = 219.1$ GPa (the largest value) for tI12-$B_6C_4O_2$. Also the (1 0 0) plane with the [0 0 1] shear stress direction and (1$\bar{1}$0) plane with [0 0 1] shear stress direction share the largest shear moduli. Furthermore, the shear moduli of tI12-$B_6C_4O_2$ within the (1 0 0) and (1$\bar{1}$0) basal planes gradually decrease with the increase of the orientation angle τ. And the smallest shear modulus is on the (1 0 0) plane with [0 1 0] shear stress direction.

3.4. Electronic properties

The electronic band structure of tI12-$B_6C_4O_2$ at ambient pressure is calculated and presented in Fig. 8. For tI12-$B_6C_4O_2$, there exist some valence bands pass through Fermi level, indicating the excellent electrical conductivity.

In order to analyze properties of chemical bonds in tI12-$B_6C_4O_2$, the partial density of state (PDOS) at ambient pressure has also been studied. Based on the hybrid orbital theory, one s orbital hybrid with three p orbitals and then form four sp^3 hybrid orbitals with the same orbital energy, suggesting that the energy ranges of s orbital and p orbitals in PDOS are identical. For the sp^2 (sp) hybrid is one s orbital hybrid with two (one) p orbitals and then form three sp^2 (two sp) hybrid orbitals, however there are one (two) p orbital leave out of hybrid, suggesting

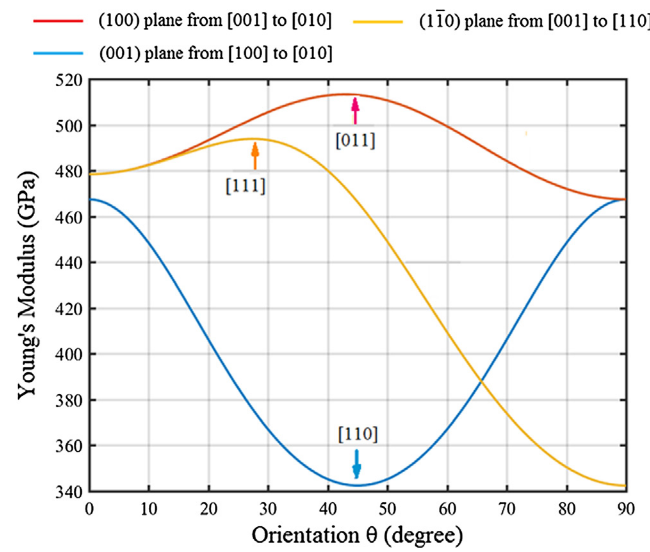

Fig. 5. Orientation dependence of Young's modulus in tI12-$B_6C_4O_2$.

that the energy ranges of p orbitals in PDOS is wider than that of s orbital. As shown in Fig. 8, s orbital and p orbitals have the overlap energy ranges in PDOS, indicating that the covalent bonds B-C and B-O in tI12-$B_6C_4O_2$ are all sp^3 hybrid bond.

4. Conclusion

In conclusion, a tetragonal B—C—O compound (tI12-$B_6C_4O_2$), which is nonisoelectronic with diamond, has been predicted using first-principles calculations. The formation enthalpies, elastic constants and phonon dispersion spectra are successfully obtained to certify their thermodynamics, mechanical and dynamic stabilities. The research

Table 1
Formulas of Young's moduli for the tensile axis within specific planes.

Tensile plane	1/E	Orientation angle τ
(0 0 1)	$S_{11}-0.25(2S_{11}-2S_{12}-S_{66})\sin^2 2\tau$	Between [h k 0] and [1 0 0]
(1 0 0)	$S_{11}\sin^4\tau + S_{33}cos^4\tau + 0.25(2S_{13} + S_{44})\sin^2 2\tau$	Between [0 k l] and [0 0 1]
(1 $\bar{1}$ 0)	$0.25(2S_{11} + 2S_{12} + S_{66})\sin^4\tau + S_{33}\cos^4\tau + 0.25(2S_{13} + S_{44})\sin^2 2\tau$	Between [h k l] and [0 0 1]

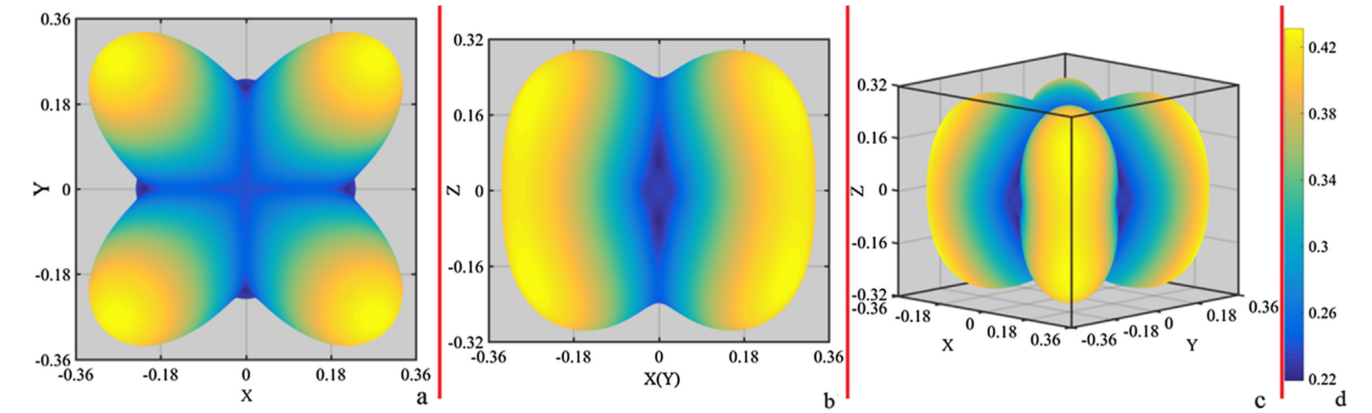

Fig. 6. Directional dependence of Poisson's ratio in *t*I12-$B_6C_4O_2$. a, b and c represent the XY plane views, ZX plane views and the stereo view, respectively. d represents the color map legend.

Table 2
Formulas of shear moduli for the shear stress direction within specific planes.

Shear plane	1/*G*	Orientation angle *τ*
(0 0 1)	S_{44}	Between [uvw] and [1 0 0]
(1 0 0)	$S_{66} + (S_{44}-S_{66})\cos^2\tau$	Between [uvw] and [0 0 1]
(1 $\bar{1}$ 0)	$2(S_{11}-S_{12})\sin^2\tau + S_{44}\cos^2\tau$	Between [uvw] and [0 0 1]

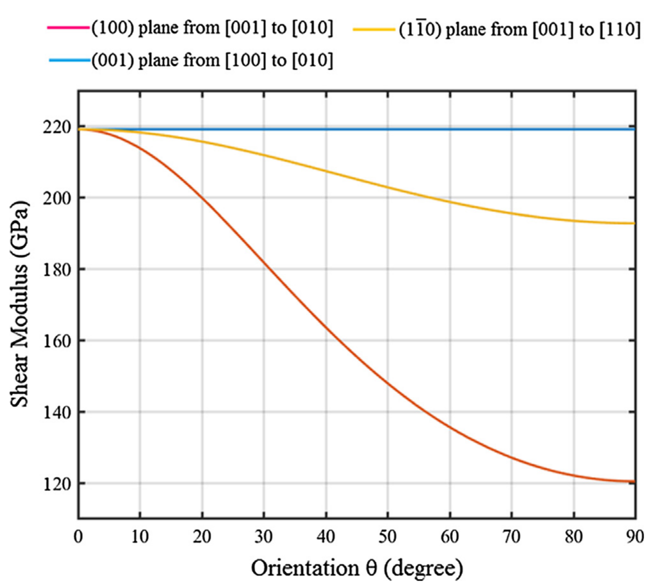

Fig. 7. Orientation dependence of shear modulus in *t*I12-$B_6C_4O_2$.

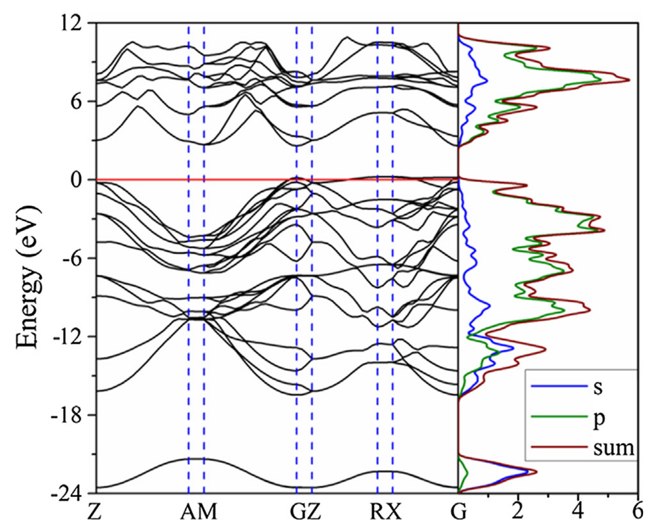

Fig. 8. Calculated band structure and PDOS for *t*I12-$B_6C_4O_2$ at ambient pressure. The Fermi level is represented by a horizontal red line.

indicates that *t*I12-$B_6C_4O_2$ has high mechanical moduli (bulk modulus, shear modulus, Young's modulus), and large hardness. The directional dependence of the Young's modulus in *t*I12-$B_6C_4O_2$ is explored. The Young's moduli with the tensile axis along specific directions are ranked as $E_{[1\,1\,0]} < E_{[1\,0\,0]} < E_{[0\,0\,1]} < E_{[1\,1\,1]} < E_{[0\,1\,1]}$. *t*I12-$B_6C_4O_2$ possesses various mechanical properties, such as ductility along [1 1 0] direction while brittleness with the directions [1 0 0] and [0 0 1]. The shear modulus of *t*I12-$B_6C_4O_2$ is the largest on the (0 0 1) basal plane, (1 0 0) plane with the [0 0 1] shear stress direction and (1 $\bar{1}$ 0) plane with [0 0 1] shear stress direction. And the smallest shear modulus is on the (1 0 0) plane with [0 1 0] shear stress direction. The calculation of mechanical properties indicates that *t*I12-$B_6C_4O_2$ is a hard material with hardness 21.9 GPa. The calculated band structure and PDOS revealed that *t*I12-$B_6C_4O_2$ is a typical for conductor and covalent bonds B-C and B-O are all sp^3 hybrid bond.

Acknowledgements

This work was supported by the National Science Foundation of China (Grant Nos. 91326203 and 51421091), and Jiangxi University of Science and Technology Scientific Research Starting Foundation (jxxjbs17053).

References

[1] L.A.J. Garvie, H. Hubert, W.T. Petuskey, P.F. McMillan, P.R. Buseck, High-Pressure, High-Temperature Syntheses in the B-C–N–O System, J. Solid State Chem. 133 (1997) 365–371.
[2] H. Hubert, L.A. Garvie, B. Devouard, P.F. McMillan, High-pressure, high-temperature syntheses of super-hard α-rhombohedral Boron-rich Solids in the BCNO, in: MRS Proceedings, Cambridge Univ Press, 1997, pp. 315–320.
[3] N. Bolotina, T. Dyuzheva, N. Bendeliani, Atomic structure of boron suboxycarbide B (C, O)$_{0.15}$5, Crystallogr. Rep. 46 (2001) 734–740.
[4] Y. Li, Q. Li, Y. Ma, B_2CO: A potential superhard material in the BCO system, EPL-Europhys. Lett. 95 (2011) 66006.
[5] M. Zhang, H. Yan, B. Zheng, Q. Wei, Influences of carbon concentration on crystal structures and ideal strengths of B_2C_XO compounds in the BCO system, Sci. Rep.-UK 5 (2015) 15481.
[6] S. Wang, A.R. Oganov, G. Qian, Q. Zhu, H. Dong, X. Dong, M.M.D. Esfahani, Novel superhard B-C–O phases predicted from first principles, Phys. Chem. Chem. Phys. 18 (2016) 1859–1863.
[7] B. Zheng, M. Zhang, C. Wang, Exploring the mechanical anisotropy and ideal strengths of tetragonal B_4CO_4, Materials 10 (2017) 128.
[8] M. Nuruzzaman, M.A. Alam, M.A.H. Shah, F. Parvin, M.A.K. Zilani, Investigation of thermodynamic stability, mechanical and electronic properties of superhard tetragonal B_4CO_4 compound: Ab initio calculations, Comput. Condensed Matter (2017).

[9] C. Liu, M. Chen, J. He, S. Yu, T. Liang, Superhard B_2CO phases derived from carbon allotropes, RSC Adv. 7 (2017) 52192–52199.
[10] C. Liu, Z. Zhao, K. Luo, M. Hu, M. Ma, J. He, Superhard orthorhombic phase of B_2CO compound, Diamond Relat. Mater. 73 (2017) 87–92.
[11] S. Zhou, J. Zhao, Two-dimensional B-C-O alloys: a promising class of 2D materials for electronic devices, Nanoscale 8 (2016) 8910–8918.
[12] Y.C. Wang, J.A. Lv, L. Zhu, Y.M. Ma, Crystal structure prediction via particle-swarm optimization, Phys. Rev. B 82 (2010) 094116.
[13] Y.C. Wang, J. Lv, L. Zhu, Y.M. Ma, CALYPSO: A method for crystal structure prediction, Comput. Phys. Commun. 183 (2012) 2063–2070.
[14] H. Wang, Y. Wang, J. Lv, Q. Li, L. Zhang, Y. Ma, CALYPSO structure prediction method and its wide application, Comput. Mater. Sci. 112 (Part B) (2016) 406–415.
[15] S.J. Clark, M.D. Segall, C.J. Pickard, P.J. Hasnip, M.J. Probert, K. Refson, M.C. Payne, First principles methods using CASTEP, Z. Kristallogr. 220 (2005) 567–570.
[16] D.M. Ceperley, B. Alder, Ground state of the electron gas by a stochastic method, Phys. Rev. Lett. 45 (1980) 566–569.
[17] J.P. Perdew, A. Zunger, Self-interaction correction to density-functional approximations for many-electron systems, Phys. Rev. B 23 (1981) 5048–5079.
[18] D. Vanderbilt, Soft self-consistent pseudopotentials in a generalized eigenvalue formalism, Phys. Rev. B 41 (1990) 7892–7895.
[19] J. Lin, A. Qteish, M. Payne, V. Heine, Optimized and transferable nonlocal separable ab initio pseudopotentials, Phys. Rev. B 47 (1993) 4174–4180.
[20] B. Montanari, N. Harrison, Lattice dynamics of TiO_2 rutile: influence of gradient corrections in density functional calculations, Chem. Phys. Lett. 364 (2002) 528–534.
[21] F. Mouhat, F.-X. Coudert, Necessary and sufficient elastic stability conditions in various crystal systems, Phys. Rev. B 90 (2014) 224104.
[22] Y.A. Freiman, H.-J. Jodl, Solid oxygen, Phys. Rep. 401 (2004) 1–228.
[23] F. Birch, Finite strain isotherm and velocities for single-crystal and polycrystalline NaCl at high pressures and 300 °K, J. Geophys. Res. Atmos. 83 (1978) 1257–1268.
[24] X.Q. Chen, H.Y. Niu, D.Z. Li, Y.Y. Li, Modeling hardness of polycrystalline materials and bulk metallic glasses, Intermetallics 19 (2011) 1275–1281.
[25] V. Tvergaard, J.W. Hutchinson, Microcracking in Ceramics Induced by Thermal Expansion or Elastic Anisotropy, J. Am. Ceram. Soc. 71 (1988) 157–166.
[26] C. Liu, M. Ma, X. Yuan, H. Sun, P. Ying, B. Xu, Z. Zhao, J. He, Metastable phases, phase transformation and properties of AlAs based on first-principle study, Comput. Mater. Sci. 128 (2017) 337–342.
[27] Y. He, R.B. Schwarz, A. Migliori, S.H. Whang, Elastic constants of single crystal γ–TiAl, J. Mater. Res. 10 (1995) 1187–1195.
[28] J.F. Nye, Physical Properties of Crystals: Their Representation by Tensors and Matrices, Oxford University Press, 1985.